

# Single Open Sites on Fe<sup>II</sup> Ions Stabilized by Coupled Metal Ions in CN-Deficient Prussian Blue Analogues for High Catalytic Activity in the Hydrolysis of Organophosphates

メタデータ	言語: English 出版者: American Chemical Society 公開日: 2021-11-01 キーワード (Ja): キーワード (En): heterogeneous catalyst, coordination polymer, defect, open metal site, hydrolysis 作成者: 山根, 真理, 田部, 博康, 川上, 正美, 田中, 寿, 川本, 徹, 山田, 裕介 メールアドレス: 所属: Osaka City University, Osaka City University, Nanomaterials Research Institute, Nanomaterials Research Institute, Nanomaterials Research Institute, Osaka City University
URL	<a href="https://ocu-omu.repo.nii.ac.jp/records/2019895">https://ocu-omu.repo.nii.ac.jp/records/2019895</a>

# Single Open Sites on Fe<sup>II</sup> Ions Stabilized by Coupled Metal Ions in CN-Deficient Prussian Blue Analogues for High Catalytic Activity in the Hydrolysis of Organophosphates

Mari Yamane, Hiroyasu Tabe, Masami Kawakami, Hisashi Tanaka,  
Tohru Kawamoto, and Yusuke Yamada

<b>Citation</b>	Inorganic Chemistry. 59(21); 16000-16009
<b>Issue Date</b>	2020-10-19
<b>Type</b>	Journal Article
<b>Textversion</b>	author
<b>Rights</b>	This document is the Accepted Manuscript version of a Published Work that appeared in final form in Inorganic Chemistry, copyright © American Chemical Society after peer review and technical editing by the publisher. To access the final edited and published work see <a href="https://doi.org/10.1021/acs.inorgchem.0c02528">https://doi.org/10.1021/acs.inorgchem.0c02528</a> .
<b>Supporting Information</b>	The Supporting Information is available free of charge at <a href="https://pubs.acs.org/doi/10.1021/acs.inorgchem.0c02528">https://pubs.acs.org/doi/10.1021/acs.inorgchem.0c02528</a> . Scanning electron microscope (SEM) images, X-ray fluorescence spectra, X-ray photoelectron spectra (XPS), nitrogen (N <sub>2</sub> ) adsorption–desorption isotherms, infrared (IR) spectra, ultraviolet–visible (UV–vis) spectra, powder X-ray diffraction (PXRD) patterns, reaction profiles, and elemental analyses data (PDF)
<b>DOI</b>	10.1021/acs.inorgchem.0c02528

Self-Archiving by Author(s)  
Placed on: Osaka City University Repository

YAMANE M, TABE H, KAWAKAMI M, TANAKA H, KAWAMOTO T, & YAMADA Y. (2020). Single Open Sites on Fe<sup>II</sup> Ions Stabilized by Coupled Metal Ions in CN-Deficient Prussian Blue Analogues for High Catalytic Activity in the Hydrolysis of Organophosphates. *Inorganic Chemistry*. 59, 16000-16009. <https://doi.org/10.1021/acs.inorgchem.0c02528>

# Single Open Sites on Fe<sup>II</sup> Ions Stabilized by Coupled Metal Ions in CN-Deficient Prussian Blue Analogues for High Catalytic Activity in the Hydrolysis of Organophosphates

Mari Yamane,<sup>†</sup> Hiroyasu Tabe,<sup>†,‡</sup> Masami Kawakami,<sup>§</sup> Hisashi Tanaka,<sup>§</sup> Tohru Kawamoto<sup>§</sup> and  
Yusuke Yamada\*<sup>†,‡</sup>

<sup>†</sup>Department of Applied Chemistry and Bioengineering, Graduate School of Engineering, Osaka  
City University, 3-3-138 Sugimoto, Sumiyoshi, Osaka 558-8585, Japan

<sup>‡</sup>Research Center of Artificial Photosynthesis (ReCAP), Osaka City University, 3-3-138  
Sugimoto, Sumiyoshi, Osaka 558-8585, Japan

<sup>§</sup>Nanomaterials Research Institute, National Institute of Advanced Industrial Science and  
Technology (AIST), 1-1-1 Higashi, Tsukuba 305-8565, Japan

**KEYWORDS:** heterogeneous catalyst, coordination polymer, defect, open metal site, hydrolysis

## ABSTRACT

CN-deficient Prussian blue analogues (PBAs),  $[M^N(H_2O)_x]_y[Fe^{II}(CN)_5(NH_3)]$  ( $M^N = Cu^{II}$ ,  $Co^{II}$  or  $Ga^{III}$ ), were synthesized and examined as a new class of heterogeneous catalysts for hydrolytic decomposition of organophosphates often used as pesticides. The active species of the CN-deficient PBAs were mainly C-bound  $Fe^{II}$  ions with exactly single open sites generated by liberation of the  $NH_3$  ligand during the catalytic reactions.  $[Cu^{II}(H_2O)_{8/3}]_{3/2}[Fe^{II}(CN)_5(NH_3)]$  showed higher catalytic activity than  $[Co^{II}(H_2O)_{8/3}]_{3/2}[Fe^{II}(CN)_5(NH_3)]$  and  $[Ga^{III}(H_2O)][Fe^{II}(CN)_5(NH_3)]$  although N-bound  $Cu^{II}$  species has been reported as less active than  $Co^{II}$  and  $Ga^{III}$  species in conventional PBAs. IR measurements of a series of the CN-deficient PBAs after the catalytic reactions clarified that a part of  $NH_3$  ligands remained on  $[Co^{II}(H_2O)_{8/3}]_{3/2}[Fe^{II}(CN)_5(NH_3)]$  and hydrogen phosphate formed as a product strongly adsorbed on the  $Fe^{II}$  ions of  $[Ga^{III}(H_2O)][Fe^{II}(CN)_5(NH_3)]$ . Hydrogen phosphate also adsorbed but weakly on the  $Fe^{II}$  ions of  $[Cu^{II}(H_2O)_{8/3}]_{3/2}[Fe^{II}(CN)_5(NH_3)]$ . These results suggest that heterogeneous catalysis of the  $Fe^{II}$  ions with single open sites were tuned by the  $M^N$  ions through metal-metal interaction.

## INTRODUCTION

Utilization of defective coordination polymers as heterogeneous catalysts attracts much attention, because active species with open sites can be intentionally created, resulting in showing unique catalysis contrast to metals or metal oxides.<sup>1-5</sup> In the defective coordination polymers, active species are metal ions with open sites usually formed by the liberation of extra ligands bound to the metal ions.<sup>6-23</sup> For example, the number of open metal sites in coordination polymers composed of ruthenium(II) ion ( $Ru^{II}$ ) and 1,3,5-benzenetricarboxylate trianion was

regulated by adding isophthalate or pyridine-3,5-dicarboxylate dianion as a second ligand, because a certain amount of extra ligand such as chloride coordinated to the Ru<sup>II</sup> ions.<sup>22,23</sup> The extra ligands are liberated to provide open sites on the Ru<sup>II</sup> ions acting as catalytic active species. The average number of open sites on Ru<sup>II</sup> ions can be controlled by changing the ratio of tri- and dianion ligands.

Another example is Prussian blue analogues (PBAs) composed of a hexacyanometallate anion ( $[M^C(CN)_6]^{n-}$ ) and a metal ion ( $M^N$ ) to form a  $M^C-CN-M^N$  framework.<sup>24-27</sup> Catalysis of PBAs has been studied for various reactions including photocatalytic water oxidation and hydrolysis of organophosphates often used as pesticides.<sup>28-47</sup> Usually, open sites acting as catalytic active sites are selectively formed on the  $M^N$  ions by liberation of the extra ligand such as water, because the number of  $M^N$  ions in a PBA is larger than that of  $[M^C(CN)_6]^{n-}$  anions to maintain charge balance, indicating that  $M^N$  ions have extra ligands to satisfy the octahedral coordination structure (Figure 1a). The catalytic properties of  $M^N$  ions can be modulated by the electronic interaction between  $M^N$  and  $M^C$  ions, resulting in the enhancement of heterogeneous catalysis. Average number of open sites formed on  $M^N$  ions can be theoretically calculated under the consideration of the valence of  $[M^C(CN)_6]^{n-}$  and  $M^N$ . However, the exact number of open sites formed on each  $M^N$  ion has yet to be precisely controlled.

We report herein the intentional creation of an open site on the C-bound Fe<sup>II</sup> ions in PBAs by using  $[Fe^{II}(CN)_5L]^{3-}$  ( $L = NH_3$  or  $H_2O$ ) instead of  $[Fe^{II}(CN)_6]^{4-}$  as a building unit (Figure 1b). The resulting CN-deficient PBAs possess exactly single open sites on the Fe<sup>II</sup> ions. The catalysis of a series of CN-deficient PBAs composed of  $[Fe^{II}(CN)_5L]^{3-}$  and various  $M^N$  ions ( $Cu^{II}$ ,  $Co^{II}$  or  $Ga^{III}$ ) are examined for organophosphate hydrolysis, because Fe<sup>II</sup> ions have been reported to show high activity for the hydrolysis reaction (Figure 1c).<sup>28</sup> The correlation between catalytic

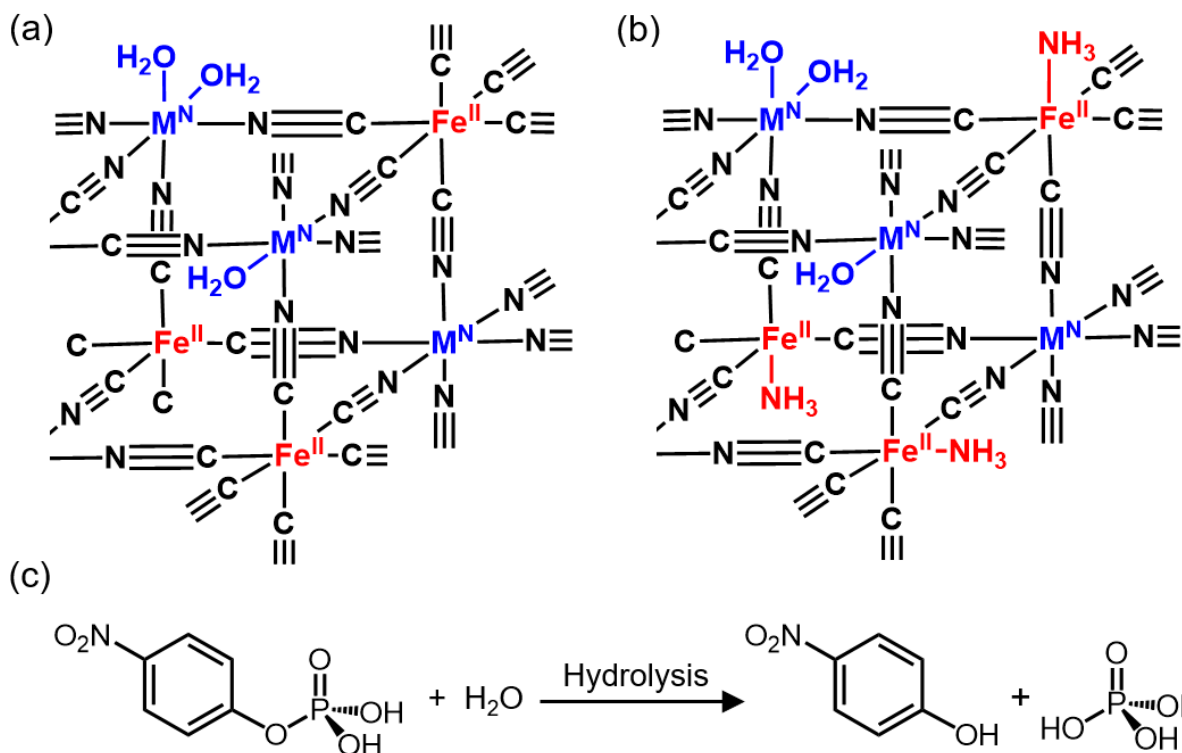


**Figure 1.** Partial structures of (a)  $[M^N(H_2O)_x]_y[Fe^{II}(CN)_6]$  ( $M^NFe$ ) and (b)  $[M^N(H_2O)_x]_y[Fe^{II}(CN)_5(NH_3)]$  ( $M^NFe-NH_3$ ) complexes. (c) The hydrolysis of *p*-nitrophenyl phosphate (*p*-NPP).

behavior and adsorbed species on the surfaces of the CN-deficient PBAs composed of various  $M^N$  ions is scrutinized.

## EXPERIMENTAL SECTION

**Materials.** Potassium ferrocyanide trihydrate, sodium pentacyanoammineferroate(II) hydrate, copper(II) nitrate trihydrate, cobalt(II) nitrate hexahydrate, gallium(III) nitrate hydrate, disodium *p*-nitrophenyl phosphate hexahydrate, *p*-nitrophenol, concentrated hydrochloric acid, concentrated nitric acid, sodium chloride, trisodium phosphate and sodium hydroxide were purchased from FUJIFILM-Wako Pure Chemical Industries Corporation. Potassium hexacyanoferrate(II) trihydrate and 4-(2-hydroxyethyl)-1-piperazineethanesulfonic acid

(HEPES) were obtained from Sigma-Aldrich Co. LLC. All chemicals were used without further purification. Purified water was provided by a water purification system, Advantec RFD210TA, where the electronic conductance was 18.2 M $\Omega$  cm.

**Synthesis of  $[\text{Cu}^{\text{II}}(\text{H}_2\text{O})_x]_y\{[\text{Fe}^{\text{II}}(\text{CN})_5(\text{NH}_3)]_n[\text{Fe}^{\text{II}}(\text{CN})_6]_{1-n}\}$  complexes ( $n = 0, 0.50, 0.83$  or  $1$ ).** An aqueous solution (3.0 mL) containing sodium pentacyanoammineferroate(II) ( $\text{Na}_3[\text{Fe}^{\text{II}}(\text{CN})_5(\text{NH}_3)]$ , 0–0.10 M) and potassium hexacyanoferrate(II) ( $\text{K}_4[\text{Fe}^{\text{II}}(\text{CN})_6]$ , 0–0.10 M) was slowly added to an aqueous solution of copper(II) nitrate (0.13 M, 4.5 mL) with vigorous stirring for 17.5 h. The formed brown precipitates were collected by centrifugation and washed with distilled water a few times. The precipitates were dried *in vacuo* for 12 h. The dried precipitates were milled using a mortar to obtain fine powder of  $[\text{Cu}^{\text{II}}(\text{H}_2\text{O})_x]_y\{[\text{Fe}^{\text{II}}(\text{CN})_5(\text{NH}_3)]_n[\text{Fe}^{\text{II}}(\text{CN})_6]_{1-n}\}$  complexes.

**Synthesis of  $[\text{Co}^{\text{II}}(\text{H}_2\text{O})_3]_2[\text{Fe}^{\text{II}}(\text{CN})_6]$  (CoFe) and  $[\text{Ga}^{\text{III}}(\text{H}_2\text{O})_{3/2}]_{4/3}[\text{Fe}^{\text{II}}(\text{CN})_6]$  (GaFe).** CoFe and GaFe was synthesized according to the literature procedure with a slight modification.<sup>28</sup> An aqueous solution of  $\text{K}_4[\text{Fe}^{\text{II}}(\text{CN})_6]$  (0.10 M, 8 mL) was slowly added to an aqueous solution of cobalt(II) nitrate or gallium(III) nitrate (0.10 M, 16 mL) with vigorous stirring for 17.5 h. The formed brown precipitates were collected by centrifugation and washed with distilled water a few times. The precipitates were dried *in vacuo* for 12 h. The dried precipitates were milled using a mortar to obtain fine powder of CoFe and GaFe.

**Synthesis of  $[\text{Co}^{\text{II}}(\text{H}_2\text{O})_{8/3}]_{3/2}[\text{Fe}^{\text{II}}(\text{CN})_5(\text{NH}_3)]$  (CoFe-NH<sub>3</sub>) and  $[\text{Ga}^{\text{III}}(\text{H}_2\text{O})][\text{Fe}^{\text{II}}(\text{CN})_5(\text{NH}_3)]$  (GaFe-NH<sub>3</sub>).** An aqueous solution of sodium pentacyanoammineferroate(II) ( $\text{Na}_3[\text{Fe}^{\text{II}}(\text{CN})_5(\text{NH}_3)]$ , 0.10 M, 8 mL) was slowly added to an aqueous solution of cobalt(II) nitrate or gallium(III) nitrate (0.10 M, 12 mL) with vigorous stirring for 17.5 h. The formed brown precipitates were collected by centrifugation and washed

with distilled water a few times. The precipitates were dried *in vacuo* for 12 h. The dried precipitates were milled using a mortar to obtain fine powder of **CoFe-NH<sub>3</sub>** and **GaFe-NH<sub>3</sub>**.

**Synthesis of [Cu<sup>II</sup>(H<sub>2</sub>O)<sub>8/3</sub>]<sub>3/2</sub>{[Fe<sup>II</sup>(CN)<sub>5</sub>(H<sub>2</sub>O)]<sub>3/4</sub>[Fe<sup>II</sup>(CN)<sub>5</sub>(NH<sub>3</sub>)]<sub>1/4</sub>}** (**CuFe-H<sub>2</sub>O**). Sodium pentacyanoaquaferroate(II) (Na<sub>3</sub>[Fe<sup>II</sup>(CN)<sub>5</sub>(H<sub>2</sub>O)]) was synthesized according to the reported procedure with a slight modification.<sup>48</sup> Na<sub>3</sub>[Fe<sup>II</sup>(CN)<sub>5</sub>(NH<sub>3</sub>)] (25 mM) in a deaerated 4-(2-hydroxyethyl)-1-piperazineethanesulfonate (HEPES) buffer solution (pH 7.2, 100 mM, 40 mL) containing 0.87 M sodium chloride was allowed to stand for 15 min under N<sub>2</sub> atmosphere with vigorous stirring. The ratio of [Fe<sup>II</sup>(CN)<sub>5</sub>(H<sub>2</sub>O)]<sup>3-</sup> and [Fe<sup>II</sup>(CN)<sub>5</sub>(NH<sub>3</sub>)]<sup>3-</sup> in the resulting solution was 3:1, as determined by IR absorption using the ATR technique, however, [Fe<sup>II</sup>(CN)<sub>5</sub>(H<sub>2</sub>O)]<sup>3-</sup> cannot be further purified by either recrystallization or chromatography due to its instability. Then, the solution containing [Fe<sup>II</sup>(CN)<sub>5</sub>(H<sub>2</sub>O)]<sup>3-</sup> was slowly added to an aqueous solution of copper(II) nitrate (0.3 M, 7.5 mL) with vigorous stirring for 17.5 h. The formed brown precipitates were collected by centrifugation and washed with distilled water a few times. The precipitates were dried *in vacuo* for 12 h. The dried precipitates were milled using a mortar to obtain fine powder of **CuFe-H<sub>2</sub>O**.

**Physical measurements.** Ultraviolet–visible (UV–vis) absorption spectra were recorded on a JASCO V–770 spectrometer. Infrared (IR) spectra were obtained on a JASCO FT/IR–6200 spectrometer with an attenuated total reflectance unit using a diamond window. The amount of ammine ligand and ammonium ion in the PBAs were calculated according to a literature procedure with slight modifications.<sup>49</sup> Powder X-ray diffraction patterns were recorded on a Shimadzu XD–3A. Incident X-ray radiation was produced by an Fe X-ray tube operating at 40 kV and 15 mA with Fe K $\alpha$  radiation ( $\lambda = 1.94 \text{ \AA}$ ). The scan rate was  $1^\circ \text{ min}^{-1}$  from  $2\theta = 20\text{--}60^\circ$ . The atomic ratio of PBAs was determined using a Shimadzu EDX–730 X-ray fluorescence



spectrometer. Inductively coupled plasma optical emission spectroscopy (ICP-OES) analyses were performed on a Shimadzu ICPE-9810. Prior to the analyses, PBAs (ca. 1 mg) were dispersed in a mixed solution of nitric acid and sulfuric acid ( $v/v = 1/1$ , 1.0 mL). The dispersion was ultrasonicated for several minutes to dissolve the PBAs. The obtained clear solutions were then diluted by adding a certain amount of 2 M nitric acid and purified water to obtain the sample solutions in the optimum concentration range for ICP-OES analyses. Inductively coupled plasma mass spectrometry (ICP-MS) analyses were performed on a PerkinElmer NexION 300D. Prior to the analyses, PBAs (5.0 mg) were dispersed in a mixed solution of nitric acid and hydrochloric acid ( $v/v = 1/1$ , 6.0 mL). The dispersion was heated using a PerkinElmer Multiwave 3000 system (1200 W) for 10 min followed by holding at the temperature for 15 min to dissolve the PBAs. The obtained clear solutions were then diluted by adding a certain amount of 2% nitric acid and purified water to obtain the sample solutions in the optimum concentration range for ICP-MS analyses. Scanning electron microscope (SEM) images of the PBAs were obtained using a JEOL JSM-6500F operated at 15 kV. X-ray photoelectron spectroscopy (XPS) analyses were performed using a Shimadzu ESCA-3400HSE. An incident radiation was Mg  $K\alpha$  X-ray (1253.6 eV) at 200 W. The samples were mounted on a stage with a double-sided carbon tape. The binding energy of each element was corrected by the C 1s peak (284.6 eV) from the carbon tape.

Nitrogen ( $N_2$ ) adsorption-desorption isotherms at  $-196\text{ }^\circ\text{C}$  were obtained with a MicrotracBEL Belsorp-mini II. Weighed samples ( $\sim 100$  mg) were used for adsorption analysis after pretreatment at  $150\text{ }^\circ\text{C}$  for 1 h *in vacuo*. The samples were exposed to  $N_2$  within a relative pressure range from 0.01 to 101.3 kPa. Adsorbed amount of  $N_2$  was calculated from the pressure change in a cell after reaching equilibrium at  $-196\text{ }^\circ\text{C}$ . The total surface area was calculated from

the Brunauer–Emmett–Teller (BET) plot. Size of mesopores and micropores were calculated by the Barrett–Joyner–Halenda (BJH) method and microporous (MP) method, respectively.

**Catalysis evaluation for the hydrolysis of organophosphates.** A typical procedure for catalysis measurements is as follows: a HEPES buffer solution (750  $\mu\text{L}$ , 100 mM, pH 6.0 or 8.3) containing disodium *p*-nitrophenyl phosphate (*p*-NPP, 25 mM) and a catalyst (0.063 mmol of Fe) in a sealed microtube was shaken at 900 rpm at 50 °C using an a Block Bath Shaker (MyBL-100S, As One, Japan). An aliquot (10  $\mu\text{L}$ ) of the reaction mixture periodically sampled was diluted with a HEPES buffer solution (2,490  $\mu\text{L}$ , 100 mM, pH 8.3) and analyzed by a UV–vis spectrophotometer. The conversion ratio of *p*-NPP at a certain reaction time was determined by the absorbance change at 400 nm ascribed to the formed *p*-nitrophenolate ion (*p*-NP,  $\varepsilon = 1.57 \times 10^4 \text{ M}^{-1} \text{ cm}$ ). Recycling performance was evaluated by adding a buffer solution containing *p*-NPP to a catalyst taken out from the reaction solution by centrifugation.

## RESULTS AND DISCUSSION

**Structure of  $[\text{M}^{\text{N}}(\text{H}_2\text{O})_x]_y[\text{Fe}^{\text{II}}(\text{CN})_5(\text{NH}_3)]$  ( $\text{M}^{\text{N}}\text{Fe-NH}_3$ ) complexes.**  $\text{Cu}^{\text{II}}$ ,  $\text{Co}^{\text{II}}$  and  $\text{Ga}^{\text{III}}$  ions were chosen as  $\text{M}^{\text{N}}$  ions of the CN-deficient PBAs because of different valence and catalytic behavior of each metal ion as reported previously.  $\text{Cu}^{\text{II}}$  ion is divalent ion with low activity for hydrolysis of *p*-nitrophenyl phosphate (*p*-NPP),  $\text{Co}^{\text{II}}$  ion is also divalent but catalytically active, and  $\text{Ga}^{\text{III}}$  is trivalent and catalytically active.<sup>28</sup>  $[\text{Cu}^{\text{II}}(\text{H}_2\text{O})_{8/3}]_{3/2}[\text{Fe}^{\text{II}}(\text{CN})_5(\text{NH}_3)]$  (**CuFe-NH<sub>3</sub>**),  $[\text{Co}^{\text{II}}(\text{H}_2\text{O})_{8/3}]_{3/2}[\text{Fe}^{\text{II}}(\text{CN})_5(\text{NH}_3)]$  (**CoFe-NH<sub>3</sub>**) and  $[\text{Ga}^{\text{III}}(\text{H}_2\text{O})][\text{Fe}^{\text{II}}(\text{CN})_5(\text{NH}_3)]$  (**GaFe-NH<sub>3</sub>**) were obtained by the reaction of  $\text{Na}_3[\text{Fe}^{\text{II}}(\text{CN})_5(\text{NH}_3)]$  with  $\text{Cu}^{\text{II}}$ ,  $\text{Co}^{\text{II}}$  and  $\text{Ga}^{\text{III}}$  ions, respectively. Similarly,  $[\text{Cu}^{\text{II}}(\text{H}_2\text{O})_3]_2[\text{Fe}^{\text{II}}(\text{CN})_6]$  (**CuFe**),  $[\text{Co}^{\text{II}}(\text{H}_2\text{O})_3]_2[\text{Fe}^{\text{II}}(\text{CN})_6]$  (**CoFe**) and  $[\text{Ga}^{\text{III}}(\text{H}_2\text{O})_{3/2}]_{4/3}[\text{Fe}^{\text{II}}(\text{CN})_6]$  (**GaFe**) were synthesized by the reaction of  $\text{K}_4[\text{Fe}^{\text{II}}(\text{CN})_6]$  with the corresponding metal ions. The scanning electron microscope (SEM) images showed that the

particles size of each PBA was 50  $\mu\text{m}$  at the largest and most of particles were less than 20  $\mu\text{m}$  (Figure S1). No shape-controlled particles were observed even at smaller particles. Insignificant contamination of  $\text{Na}^+$  and  $\text{K}^+$  ions in the PBAs was assured by inductively coupled plasma optical emission spectroscopy (ICP-OES) and X-ray fluorescence spectroscopy, where the molar ratios of  $\text{Na}/\text{Fe}$  and  $\text{K}/\text{Fe}$  are lower than 0.0035 and 0.026, respectively (Figure S2 and Table S1).

X-ray photoelectron spectroscopy (XPS) measurements of **CuFe-NH<sub>3</sub>** and **CuFe** were performed for the energy regions of Cu 2p, Fe 2p, O 1s and N 1s (Figure S3). The values for binding energy of Cu 2p<sub>3/2</sub> of **CuFe-NH<sub>3</sub>** and **CuFe** were 933.8 eV and 933.2 eV, respectively, which are close to the typical values for the Cu<sup>II</sup> species (933.5 eV).<sup>50</sup> The binding energy of Fe 2p<sub>3/2</sub> peaks were found at 708.7 eV and 709.1 eV for **CuFe-NH<sub>3</sub>** and **CuFe**, respectively, which are also comparable to the typical binding energy of Fe<sup>II</sup> species (709.1 eV).<sup>50</sup> These results suggest that the involvement of NH<sub>3</sub> ligands hardly affected the oxidation states of Cu<sup>II</sup> and Fe<sup>II</sup> ions. The binding energy of O 1s in **CuFe-NH<sub>3</sub>** was 532.5 eV, which is virtually the same to that of **CuFe** (532.2 eV). The binding energy of N 1s in **CuFe-NH<sub>3</sub>** (397.9 eV) was also similar to that in **CuFe** (398.3 eV) even in the presence of NH<sub>3</sub> ligands, because the peaks for N 1s in CN<sup>-</sup> and NH<sub>3</sub> ligands (397.7 and 399.0 eV, respectively, according to the literature) are overlapped, but the peak was hardly deconvoluted.<sup>51</sup>

The bridging structures of Fe<sup>II</sup>-CN-M<sup>N</sup> in **M<sup>N</sup>Fe-NH<sub>3</sub>** complexes were confirmed by infrared (IR) spectroscopy. The CN-stretching bands ( $\nu_{\text{CN}}$ ) of **CuFe-NH<sub>3</sub>**, **CoFe-NH<sub>3</sub>** and **GaFe-NH<sub>3</sub>** appeared at 2094, 2084 and 2106  $\text{cm}^{-1}$ , respectively, which were shifted from that of  $\text{K}_3[\text{Fe}^{\text{II}}(\text{CN})_5(\text{NH}_3)]$  (2038  $\text{cm}^{-1}$ ) in the higher wavenumber region (Figure 2). Such higher wavenumber shift evidenced the formation of Fe<sup>II</sup>-CN-M<sup>N</sup> structures, because the electron density of an antibonding orbital of CN ligand was reduced by the additional coordination to M<sup>N</sup>

ions.<sup>52</sup> Also, the wavenumbers of  $\nu_{\text{CN}}$  similar to those of corresponding **CuFe**, **CoFe** and **GaFe** appeared at 2096, 2084 and 2117  $\text{cm}^{-1}$ , respectively, supported the  $\text{Fe}^{\text{II}}\text{-CN-M}^{\text{N}}$  formation without ligand isomerization (Figure 2).<sup>52</sup> The wavenumber of  $\nu_{\text{CN}}$  of **GaFe-NH<sub>3</sub>** (2106  $\text{cm}^{-1}$ ) lower than that of **GaFe** (2117  $\text{cm}^{-1}$ ) by 11  $\text{cm}^{-1}$  resulted from a partial oxidation of Fe ions in **GaFe** as reported previously,<sup>53</sup> indicating that the valence of Fe ions is +2 in **GaFe-NH<sub>3</sub>**. Also, ammine ligand coordination in **CuFe-NH<sub>3</sub>**, **CoFe-NH<sub>3</sub>** and **GaFe-NH<sub>3</sub>** was confirmed by the peaks at 1344, 1269 and 1270  $\text{cm}^{-1}$ , respectively, assigned to H–N–H bending vibration ( $\delta_{\text{HNNH}}$ ), which were not observed for **CuFe**, **CoFe** and **GaFe**.<sup>54</sup> The peaks at around 1400  $\text{cm}^{-1}$  observed for **CuFe-NH<sub>3</sub>**, **CoFe-NH<sub>3</sub>** and **GaFe-NH<sub>3</sub>** can be assigned to  $\delta_{\text{HNNH}}$  of ammonium ion ( $\text{NH}_4^+$ ) trapped in the interstitial sites of PBAs.<sup>54</sup>  $\text{NH}_4^+$  could be formed by partial replacement of  $\text{NH}_3$  to  $\text{H}_2\text{O}$  ligands during synthesis in an aqueous solution (*vide infra*).

Nitrogen ( $\text{N}_2$ ) adsorption-desorption isotherms of PBAs were performed to investigate their porous structures (Figure S4). The total surface areas were calculated from the Brunauer–Emmett–Teller (BET) method (Table 1). Homogeneous distribution of micropores (0.5–0.7 nm) formed by the cubic lattice structure of PBAs were determined by the microporous (MP) method. Type IV isotherms observed for a series of PBAs suggest the presence of mesopores in the sizes of 3–10 nm as determined by the Barrett–Joyner–Halenda (BJH) method. The mesopores in this size range are formed by the gaps among PBA particles, as reported previously.<sup>28</sup>

The powder X-ray diffraction (PXRD) patterns obtained for  $\text{M}^{\text{N}}\text{Fe-NH}_3$  complexes were assignable to cubic structure (Figure 3a, c, e). The cell parameters obtained for  $\text{M}^{\text{N}} = \text{Cu}$ ,  $\text{Co}$  and  $\text{Ga}$  were  $a = 10.00$ ,  $9.94$  and  $10.04$  Å, respectively. The  $a$  values were comparable to those of corresponding  $\text{M}^{\text{N}}\text{Fe}$  complexes without open sites on  $\text{Fe}^{\text{II}}$  ions, where  $a = 9.95$ ,  $10.10$  and  $10.02$  Å for  $\text{M}^{\text{N}} = \text{Cu}$ ,  $\text{Co}$  and  $\text{Ga}$ , respectively (Figure 4b, d, f). Broader peaks observed for

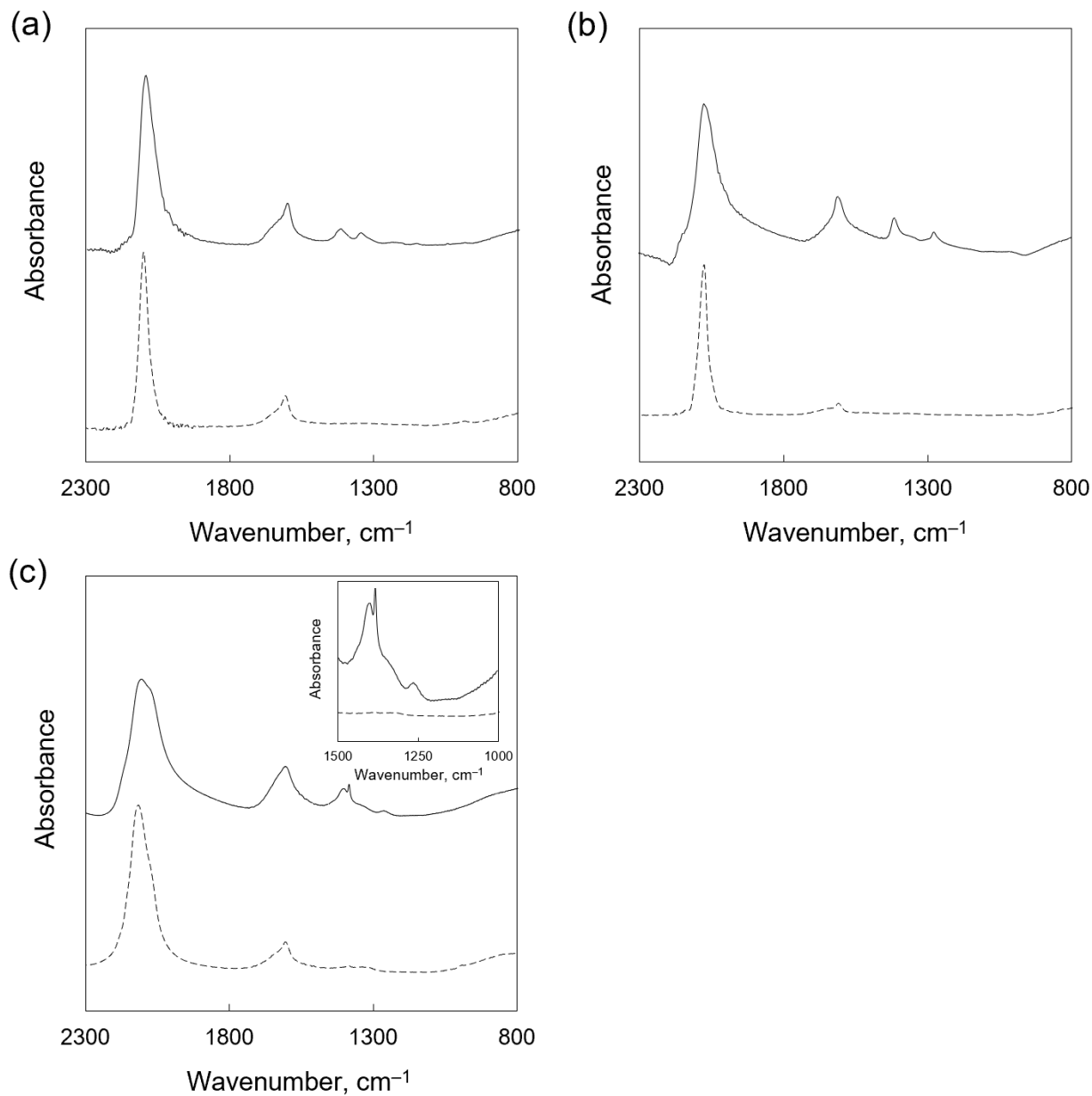


**Figure 2.** Infrared spectra of (a) [Cu<sup>II</sup>(H<sub>2</sub>O)<sub>8/3</sub>]<sub>3/2</sub>[Fe<sup>II</sup>(CN)<sub>5</sub>(NH<sub>3</sub>)] (**CuFe-NH<sub>3</sub>**, solid line) and [Cu<sup>II</sup>(H<sub>2</sub>O)<sub>2</sub>]<sub>3/2</sub>[Fe<sup>II</sup>(CN)<sub>6</sub>] (**CuFe**, broken line), (b) [Co<sup>II</sup>(H<sub>2</sub>O)<sub>8/3</sub>]<sub>3/2</sub>[Fe<sup>II</sup>(CN)<sub>5</sub>(NH<sub>3</sub>)] (**CoFe-NH<sub>3</sub>**, solid line) and [Co<sup>II</sup>(H<sub>2</sub>O)<sub>2</sub>]<sub>3/2</sub>[Fe<sup>II</sup>(CN)<sub>6</sub>] (**CoFe**, broken line), and (c) [Ga<sup>III</sup>(H<sub>2</sub>O)][Fe<sup>II</sup>(CN)<sub>5</sub>(NH<sub>3</sub>)] (**GaFe-NH<sub>3</sub>**, solid line) and [Ga<sup>III</sup>(H<sub>2</sub>O)<sub>3/2</sub>]<sub>4/3</sub>[Fe<sup>II</sup>(CN)<sub>6</sub>] (**GaFe**, broken line). Magnified views of δ<sub>HNH</sub> region (1000–1500 cm<sup>-1</sup>) are shown in the insets.

**Table 1.** Total surface areas obtained by the Brunauer–Emmett–Teller (BET) method, pore diameters obtained by the Barrett–Joyner–Halenda (BJH) method and the microporous (MP) method of a series of PBAs calculated from their N<sub>2</sub> adsorption-desorption isotherms

PBA	Total surface area, m <sup>2</sup> g <sup>-1</sup>	Mesopore diameter, nm	Micropore diameter, nm
<b>CuFe-NH<sub>3</sub></b>	77	7.0	0.7
<b>CuFe</b>	101	10.2	0.7
<b>CuFe-H<sub>2</sub>O</b>	32	4.6	0.7
<b>CoFe-NH<sub>3</sub></b>	50	5.3	0.7
<b>CoFe</b>	284	10.8	0.7
<b>GaFe-NH<sub>3</sub></b>	179	3.2	0.6
<b>GaFe</b>	393	3.5	0.8

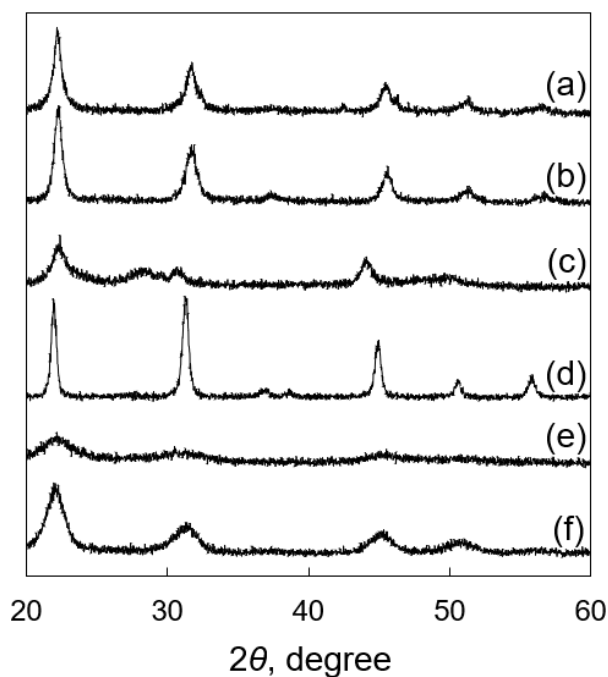


**Figure 3.** Powder X-ray diffraction patterns of (a) [Cu<sup>II</sup>(H<sub>2</sub>O)<sub>8/3</sub>]<sub>3/2</sub>[Fe<sup>II</sup>(CN)<sub>5</sub>(NH<sub>3</sub>)] (**CuFe-NH<sub>3</sub>**), (b) [Cu<sup>II</sup>(H<sub>2</sub>O)<sub>2</sub>]<sub>3/2</sub>[Fe<sup>II</sup>(CN)<sub>6</sub>] (**CuFe**), (c) [Co<sup>II</sup>(H<sub>2</sub>O)<sub>8/3</sub>]<sub>3/2</sub>[Fe<sup>II</sup>(CN)<sub>5</sub>(NH<sub>3</sub>)] (**CoFe-NH<sub>3</sub>**), (d) [Co<sup>II</sup>(H<sub>2</sub>O)<sub>2</sub>]<sub>3/2</sub>[Fe<sup>II</sup>(CN)<sub>6</sub>] (**CoFe**), (e) [Ga<sup>III</sup>(H<sub>2</sub>O)]<sub>4/3</sub>[Fe<sup>II</sup>(CN)<sub>5</sub>(NH<sub>3</sub>)] (**GaFe-NH<sub>3</sub>**) and (f) [Ga<sup>III</sup>(H<sub>2</sub>O)<sub>3/2</sub>]<sub>4/3</sub>[Fe<sup>II</sup>(CN)<sub>6</sub>] (**GaFe**).

$M^N\text{Fe-NH}_3$  complexes, especially for  $\text{GaFe-NH}_3$ , than those of  $M^N\text{Fe}$  complexes resulted from the low crystallinity of  $M^N\text{Fe-NH}_3$  complexes due to the local disorder originated from partial deficiencies of  $\text{CN}^-$  ligands. However, the shift of  $\nu_{\text{CN}}$  and microporous structures determined by the  $\text{N}_2$  adsorption-desorption isotherms indicate the formation of  $M^N\text{Fe-NH}_3$  complexes having cubic lattice structures without extended defects.

**Catalysis of  $[M^N(\text{H}_2\text{O})_x]_y[\text{Fe}^{\text{II}}(\text{CN})_5(\text{NH}_3)]$  complexes for Hydrolysis of *p*-Nitrophenyl Phosphate.** Catalytic activity of  $M^N\text{Fe}$  and  $M^N\text{Fe-NH}_3$  complexes for hydrolysis of *p*-nitrophenyl phosphate (*p*-NPP) was examined at 50 °C in a 4-(2-hydroxyethyl)-1-piperazineethanesulfonate (HEPES) buffer solution (100 mM, pH 8.3, 0.75 mL) containing metal complexes (0.063 mmol of Fe) and *p*-NPP (25 mM). The yield of the hydrolysis product, *p*-nitrophenolate ion (*p*-NP), was determined by characteristic absorbance change at 400 nm (Figure S5). No catalytic activity was observed for  $[\text{Fe}^{\text{II}}(\text{CN})_6]^{4-}$  and  $[\text{Fe}^{\text{II}}(\text{CN})_5(\text{NH}_3)]^{3-}$  dissolved in the buffer solutions (Figure 4). The IR spectrum of an aqueous solution containing  $[\text{Fe}^{\text{II}}(\text{CN})_5(\text{NH}_3)]^{3-}$  reacted with hydrogen phosphate indicates the absence of  $\delta_{\text{HNH}}$  peak at 1255  $\text{cm}^{-1}$ , suggesting that the open  $\text{Fe}^{\text{II}}$  sites formed during the reaction (Figure S6). However, the peaks at 1078  $\text{cm}^{-1}$  assignable to the PO stretching vibration ( $\nu_{\text{PO}}$ ) appeared, suggesting the coordination of hydrogen phosphate to the  $\text{Fe}^{\text{II}}$  ions.<sup>55,56</sup> Thus, tuning of electronic properties of  $\text{Fe}^{\text{II}}$  ions by  $M^N$  ions through  $\text{CN}^-$  ligand is essential to suppress the product inhibition by hydrogen phosphate.

The higher conversion ratios and initial reaction rates for 1 h ( $v_0$ ) were observed for the reaction solutions containing **CoFe** (28% for 24 h and  $0.3 \times 10^{-3} \text{ mol L}^{-1} \text{ h}^{-1}$ ) and **GaFe** (26% for 24 h and  $0.3 \times 10^{-3} \text{ mol L}^{-1} \text{ h}^{-1}$ ) compared with those containing **CuFe** (5% for 24 h and  $0.1 \times 10^{-3} \text{ mol L}^{-1} \text{ h}^{-1}$ ), indicating that the N-bound  $\text{Co}^{\text{II}}$  and  $\text{Ga}^{\text{III}}$  ions act as the active species,

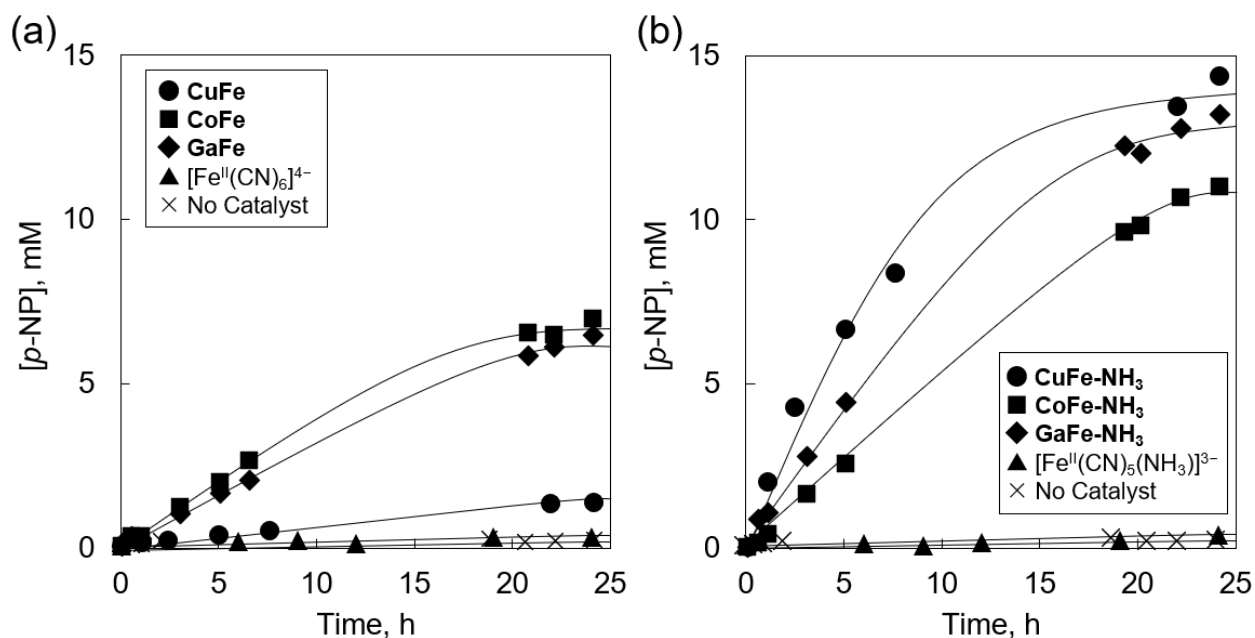


**Figure 4.** Time profiles of the *p*-nitrophenolate ion (*p*-NP) formation in a HEPES buffer solution (100 mM, 0.75 mL, pH 8.3, 50 °C) containing disodium *p*-nitrophenyl phosphate (*p*-NPP, 25 mM) in the presence of (a)  $[\text{Cu}^{\text{II}}(\text{H}_2\text{O})_3]_2[\text{Fe}^{\text{II}}(\text{CN})_6]$  (**CuFe**),  $[\text{Co}^{\text{II}}(\text{H}_2\text{O})_2]_{3/2}[\text{Fe}^{\text{II}}(\text{CN})_6]$  (**CoFe**),  $[\text{Ga}^{\text{III}}(\text{H}_2\text{O})_{3/2}]_{4/3}[\text{Fe}^{\text{II}}(\text{CN})_6]$  (**GaFe**) and hexacyanoferrate ion ( $[\text{Fe}^{\text{II}}(\text{CN})_6]^{4-}$ ), or (b)  $[\text{Cu}^{\text{II}}(\text{H}_2\text{O})_{8/3}]_{3/2}[\text{Fe}^{\text{II}}(\text{CN})_5(\text{NH}_3)]$  (**CuFe-NH<sub>3</sub>**),  $[\text{Co}^{\text{II}}(\text{H}_2\text{O})_{8/3}]_{3/2}[\text{Fe}^{\text{II}}(\text{CN})_5(\text{NH}_3)]$  (**CoFe-NH<sub>3</sub>**),  $[\text{Ga}^{\text{III}}(\text{H}_2\text{O})][\text{Fe}^{\text{II}}(\text{CN})_5(\text{NH}_3)]$  (**GaFe-NH<sub>3</sub>**) and pentacyanoammineferrate ion ( $[\text{Fe}^{\text{II}}(\text{CN})_5(\text{NH}_3)]^{3-}$ ).

however,  $\text{Cu}^{\text{II}}$  ions are inactive (Figure 4a). **CuFe-NH<sub>3</sub>** showed the higher catalytic activity compared with **CuFe**. The conversion ratio and  $v_0$  value observed for **CuFe-NH<sub>3</sub>** were 58% for 24 h and  $2.0 \times 10^{-3} \text{ mol L}^{-1} \text{ h}^{-1}$ , respectively, suggesting that the open  $\text{Fe}^{\text{II}}$  sites were successfully created during the catalytic reaction. The conversion ratios and  $v_0$  values observed for **CoFe-NH<sub>3</sub>** (44% for 24 h and  $0.4 \times 10^{-3} \text{ mol L}^{-1} \text{ h}^{-1}$ ) and **GaFe-NH<sub>3</sub>** (53% for 24 h and  $1.0 \times 10^{-3} \text{ mol L}^{-1} \text{ h}^{-1}$ ) were higher than those for **CoFe** and **GaFe**, suggesting that the  $\text{Fe}^{\text{II}}$  ions contribute to *p*-NPP hydrolysis (Figure 4b). However, the conversion ratios and  $v_0$  values for



**CoFe-NH<sub>3</sub>** and **GaFe-NH<sub>3</sub>** were lower than those of **CuFe-NH<sub>3</sub>**. These results imply that the catalytic properties of open Fe<sup>II</sup> sites of **CuFe-NH<sub>3</sub>**, **CoFe-NH<sub>3</sub>** and **GaFe-NH<sub>3</sub>** were not the same.

Repetitive catalysis experiments using **CuFe-NH<sub>3</sub>** indicated that the conversion ratios (24 h) obtained for the reactions were 42, 13, 12 and 11% at the 1<sup>st</sup> to 4<sup>th</sup> runs, respectively (Figure S7). The conversion ratio at the 2<sup>nd</sup> run was lower than that at the 1<sup>st</sup> run. No further decrease in conversion ratios were observed at the 3<sup>rd</sup> and 4<sup>th</sup> runs. A possible reason for the deceleration was structural deformation of **CuFe-NH<sub>3</sub>**, however, virtually the same PXRD patterns of **CuFe-NH<sub>3</sub>** before and after catalytic hydrolysis strongly support no degradation of **CuFe-NH<sub>3</sub>** (Figure S8). Thus, product inhibition of the Fe<sup>II</sup> ions would be a reason for deceleration.

**Adsorbed Species on Open Sites of Fe<sup>II</sup> Ions in [M<sup>N</sup>(H<sub>2</sub>O)<sub>x</sub>]<sub>y</sub>[Fe<sup>II</sup>(CN)<sub>5</sub>(NH<sub>3</sub>)] Complexes After the Reaction.** The liberation of NH<sub>3</sub> ligands from **CuFe-NH<sub>3</sub>** during the catalytic reaction was confirmed by ex situ IR spectroscopy. The IR measurement of **CuFe-NH<sub>3</sub>** after the reaction clarified that the strength of the most characteristic peak at 1348 cm<sup>-1</sup> ascribed to  $\delta_{\text{HNH}}$  decreased by ~85% compared with that of fresh **CuFe-NH<sub>3</sub>**, suggesting that open Fe<sup>II</sup> sites successfully formed during the catalytic reaction (Figure 5a).<sup>28</sup> Instead, the peaks at 1014 cm<sup>-1</sup> and around 989 cm<sup>-1</sup> assignable to  $\nu_{\text{PO}}$  appeared for **CuFe-NH<sub>3</sub>** after the reaction, indicating the adsorption of hydrogen phosphate.<sup>55,56</sup> The adsorbed hydrogen phosphate in **CuFe** and **CuFe-NH<sub>3</sub>** after the reactions were more directly quantified by inductively coupled plasma mass spectrometry (ICP-MS). The molar ratio of P and Fe in **CuFe-NH<sub>3</sub>** after the catalytic hydrolysis was 0.12, which was six times higher than that in **CuFe** (0.021, Table S2). These results suggest that hydrogen phosphate formed by the *p*-NPP hydrolysis preferably bound to the open Fe<sup>II</sup> sites in **CuFe-NH<sub>3</sub>** (Figure 6).

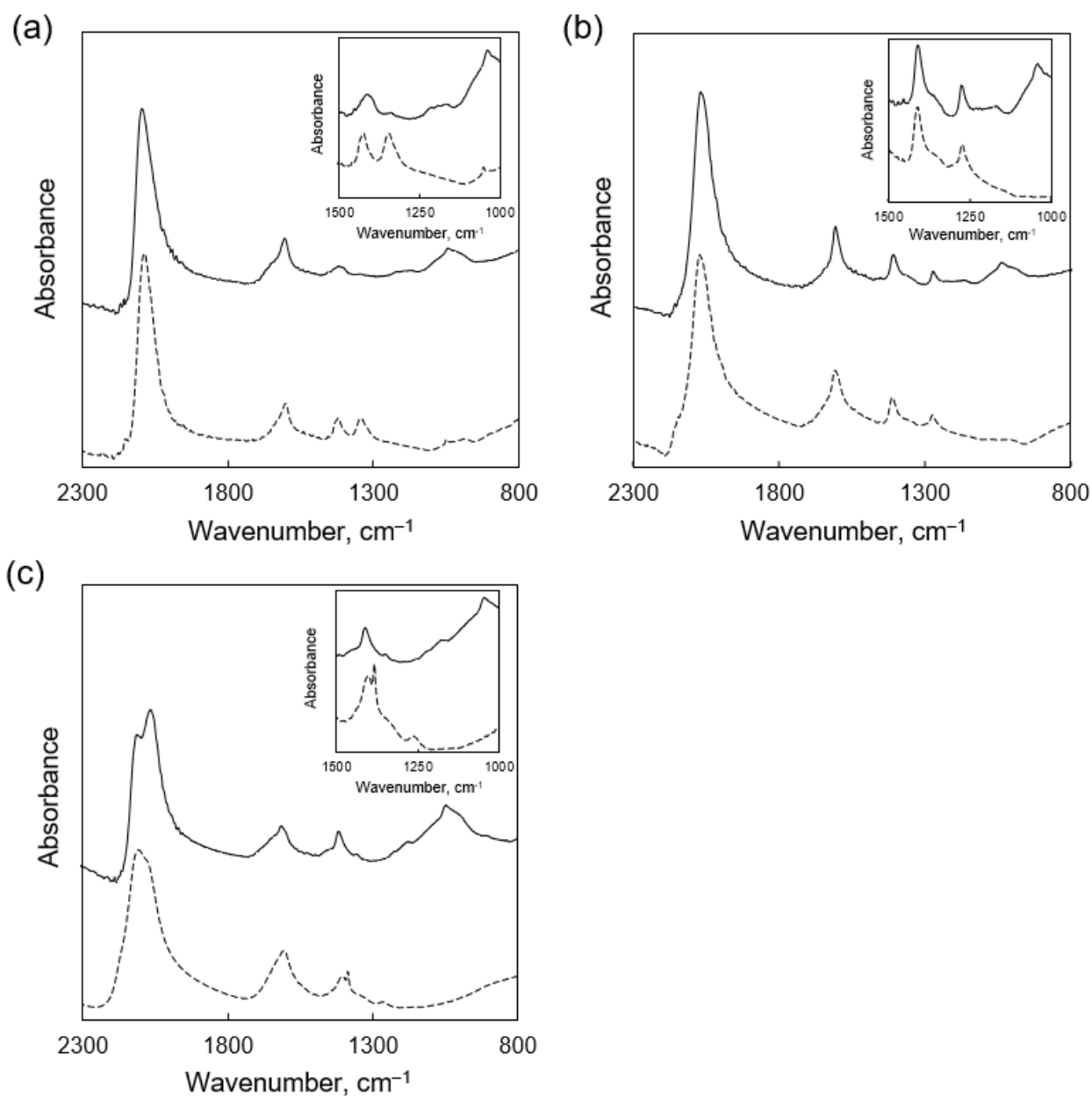


**Figure 5.** Infrared (IR) spectra of (a) [Cu<sup>II</sup>(H<sub>2</sub>O)<sub>8/3</sub>]<sub>3/2</sub>[Fe<sup>II</sup>(CN)<sub>5</sub>(NH<sub>3</sub>)] (**CuFe-NH<sub>3</sub>**), (b) [Co<sup>II</sup>(H<sub>2</sub>O)<sub>8/3</sub>]<sub>3/2</sub>[Fe<sup>II</sup>(CN)<sub>5</sub>(NH<sub>3</sub>)] (**CoFe-NH<sub>3</sub>**) and (c) [Ga<sup>III</sup>(H<sub>2</sub>O)][Fe<sup>II</sup>(CN)<sub>5</sub>(NH<sub>3</sub>)] (**GaFe-NH<sub>3</sub>**) before (broken lines) and after (solid lines) catalytic hydrolysis of disodium *p*-nitrophenyl phosphate (*p*-NPP, 25 mM) in a HEPES buffer solution (100 mM, 0.75 mL, 50 °C) for 24 h. Magnified views of δ<sub>HNH</sub> and ν<sub>PO</sub> region (1000–1500 cm<sup>-1</sup>) are shown in the insets.

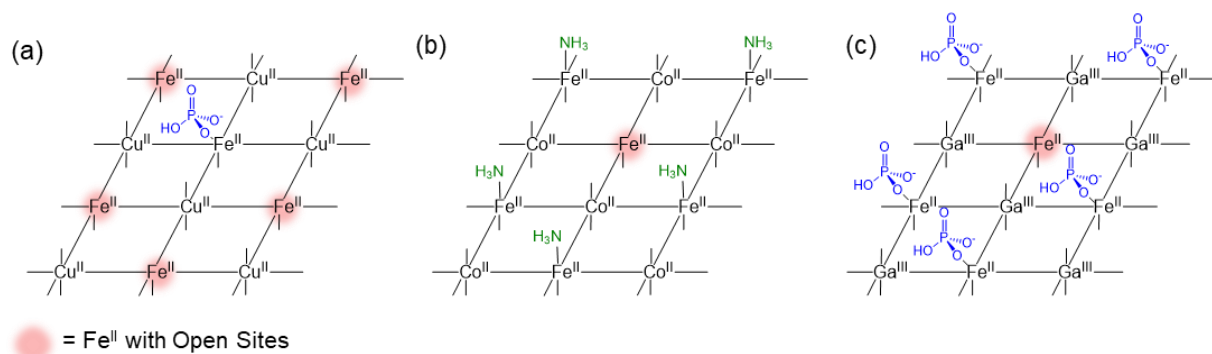


**Figure 6.** Schematic drawing of difference of adsorbed species on  $[M^N(H_2O)_x]_y[Fe^{II}(CN)_5(NH_3)]$  ( $M^N Fe-NH_3$ ) complexes ( $M^N =$  (a)  $Cu^{II}$ , (b)  $Co^{II}$  or (c)  $Ga^{III}$ ).

Adsorbed species on the surfaces of **CoFe-NH<sub>3</sub>** and **GaFe-NH<sub>3</sub>** after the reaction were also investigated by IR spectroscopy. The IR spectrum of **CoFe-NH<sub>3</sub>** after the catalytic hydrolysis showed that the  $\delta_{HNH}$  and  $\nu_{PO}$  peaks appeared at  $1262\text{ cm}^{-1}$  and  $1038\text{ cm}^{-1}$ , respectively (Figure 5b), however, no peak assignable to  $\nu_{PO}$  was observed for **CoFe** after the reaction (Figure S9a). Thus, limited liberation of  $NH_3$  ligand in **CoFe-NH<sub>3</sub>** suppressed the interaction with substrates, resulting in low catalytic activity. The IR spectrum of **GaFe-NH<sub>3</sub>** after the reaction showing strong  $\nu_{PO}$  peak appeared at  $1037\text{ cm}^{-1}$  indicated the adsorption of hydrogen phosphate bond (Figure 5c). On the other hand, much weaker  $\nu_{PO}$  peak observed for **GaFe** after the reaction indicated that hydrogen phosphate mainly adsorbed on the  $Fe^{II}$  not  $Ga^{III}$  ions of **GaFe-NH<sub>3</sub>** (Figure S9b). The  $\nu_{CN}$  peak of **GaFe-NH<sub>3</sub>** appeared at  $2066\text{ cm}^{-1}$  after the reaction is attributed to a contaminant, as reported previously.<sup>51</sup> The  $Fe^{II}$  ions with enhanced Lewis acidity by  $Co^{II}$  and  $Ga^{III}$  ions favors interaction with hydrogen phosphate and/or ammonia, which decelerate the catalytic reactions (Figure 6).<sup>28</sup> Thus, the metal ions coupled with  $Fe^{II}$  ions with single open sites in CN-deficient PBAs precisely regulated the catalysis and adsorption properties of the  $Fe^{II}$  ions.

**Liability of  $NH_3$  Compared with That of  $H_2O$  at Different pH values.** Open  $Fe^{II}$  sites formed during the catalytic reaction are active sites, thus, liberation of  $NH_3$  ligands is important

to achieve high catalytic activity. Lability of NH<sub>3</sub> ligand in **CuFe-NH<sub>3</sub>** was confirmed by catalysis comparison with **CuFe-H<sub>2</sub>O** which mainly possesses H<sub>2</sub>O as the extra ligand instead of NH<sub>3</sub>. **CuFe-H<sub>2</sub>O** was prepared by mixing an aqueous solution of Na<sub>3</sub>[Fe<sup>II</sup>(CN)<sub>5</sub>(H<sub>2</sub>O)], which was prepared from Na<sub>3</sub>[Fe<sup>II</sup>(CN)<sub>5</sub>(NH<sub>3</sub>)] according to reported procedure, with that of copper(II) nitrate.<sup>48</sup> Insignificant contamination of Na<sup>+</sup> ions was confirmed by the ICP-OES analysis, in which the molar ratio of Na/Fe was 0.021 (Table S1). The IR spectra of obtained precipitate indicated that nearly 75% of NH<sub>3</sub> was replaced with water to provide [Cu<sup>II</sup>(H<sub>2</sub>O)<sub>8/3</sub>]<sub>3/2</sub>{[Fe<sup>II</sup>(CN)<sub>5</sub>(H<sub>2</sub>O)]<sub>3/4</sub>[Fe<sup>II</sup>(CN)<sub>5</sub>(NH<sub>3</sub>)]<sub>1/4</sub>} (Figure S10).<sup>48</sup> On the other hand, the  $\nu_{\text{CN}}$  peak of **CuFe-H<sub>2</sub>O** appeared at 2094 cm<sup>-1</sup>, which is comparable to those of **CuFe-NH<sub>3</sub>** and **CuFe** (2094 and 2096 cm<sup>-1</sup>, respectively), supports the formation of bridging structures of Fe<sup>II</sup>-CN-M<sup>N</sup> with cubic lattice structure. However, slightly broader PXRD peaks assignable to cubic structure (Figure S11) and smaller total surface areas calculated from the N<sub>2</sub> adsorption-desorption measurements (Table 1) compared with those of **CuFe-NH<sub>3</sub>** suggests the low crystallinity of **CuFe-H<sub>2</sub>O**.

The catalytic hydrolysis of *p*-NPP (25 mM) was examined at 50 °C in a HEPES buffer solution (100 mM, pH 8.3, 0.75 mL) containing **CuFe-NH<sub>3</sub>** or **CuFe-H<sub>2</sub>O** (0.063 mmol of Fe). **CuFe-NH<sub>3</sub>** and **CuFe-H<sub>2</sub>O** showed very similar reaction profiles in the reaction solutions of both pH 6.0 and 8.3 (Figure 7). These results suggest that open Fe<sup>II</sup> ions acting as catalytic active species were successfully created on **CuFe-NH<sub>3</sub>** and **CuFe-H<sub>2</sub>O** irrespective of their crystallinity and solution pH.

**Concentration Effect of Fe<sup>II</sup> ions with Single Open Sites on Catalysis.** The concentration of Fe<sup>II</sup> ions with open sites were precisely tuned by concomitant use of [Fe<sup>II</sup>(CN)<sub>5</sub>(NH<sub>3</sub>)]<sup>3-</sup> and [Fe<sup>II</sup>(CN)<sub>6</sub>]<sup>4-</sup> as building blocks. [Cu<sup>II</sup>(H<sub>2</sub>O)<sub>x</sub>]<sub>y</sub>{[Fe<sup>II</sup>(CN)<sub>5</sub>(NH<sub>3</sub>)]<sub>n</sub>[Fe<sup>II</sup>(CN)<sub>6</sub>]<sub>1-n</sub>} complexes (n =

0, 0.50, 0.83 or 1) were synthesized by mixing an aqueous solution containing the various ratios of  $[\text{Fe}^{\text{II}}(\text{CN})_5(\text{NH}_3)]^{3-}$  and  $[\text{Fe}^{\text{II}}(\text{CN})_6]^{4-}$  and that containing copper(II) nitrate. Similar PXRD patterns of  $[\text{Cu}^{\text{II}}(\text{H}_2\text{O})_x]_y\{[\text{Fe}^{\text{II}}(\text{CN})_5(\text{NH}_3)]_n[\text{Fe}^{\text{II}}(\text{CN})_6]_{1-n}\}$  complexes are ascribed to the cubic structure (Figure S12).

Catalytic hydrolysis of *p*-NPP was examined in a HEPES buffer solution (100 mM, pH 6.0, 0.75 mL) containing  $[\text{Cu}^{\text{II}}(\text{H}_2\text{O})_x]_y\{[\text{Fe}^{\text{II}}(\text{CN})_5(\text{NH}_3)]_n[\text{Fe}^{\text{II}}(\text{CN})_6]_{1-n}\}$  complexes (0.063 mmol of

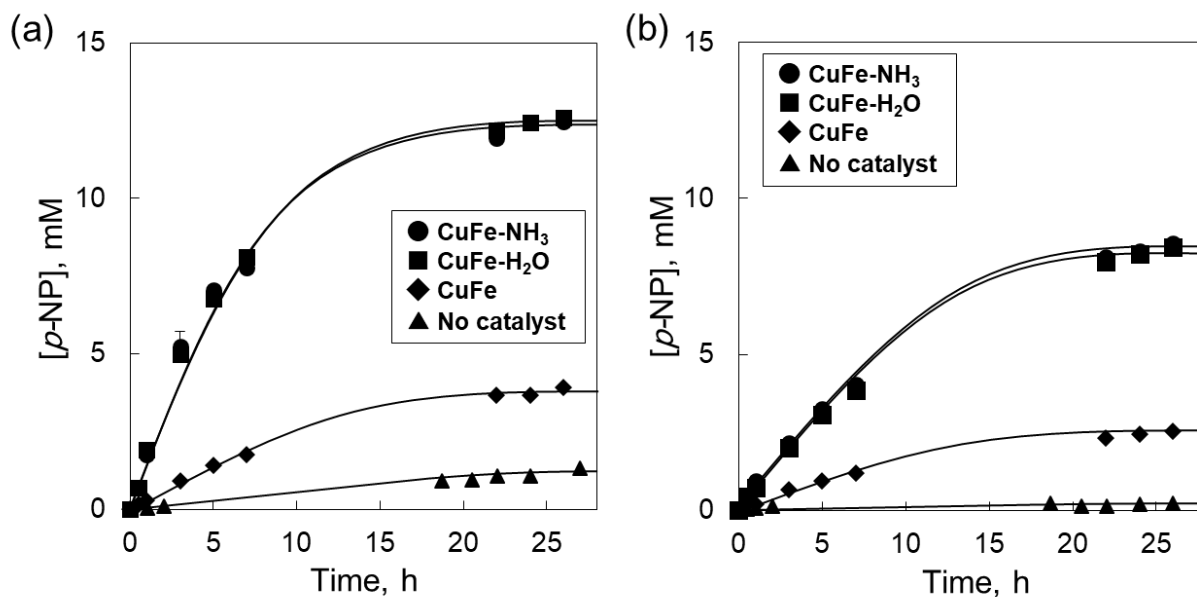


**Figure 7.** Time profiles of the *p*-nitrophenolate ion (*p*-NP) formation in a HEPES buffer solution (100 mM, 0.75 mL, 50 °C) containing disodium *p*-nitrophenyl phosphate (*p*-NPP, 25 mM) in the absence and presence of  $[\text{Cu}^{\text{II}}(\text{H}_2\text{O})_{8/3}]_{3/2}[\text{Fe}^{\text{II}}(\text{CN})_5(\text{NH}_3)]$  (**CuFe-NH<sub>3</sub>**),  $[\text{Cu}^{\text{II}}(\text{H}_2\text{O})_{8/3}]_{3/2}\{[\text{Fe}^{\text{II}}(\text{CN})_5(\text{H}_2\text{O})]_{3/4}[\text{Fe}^{\text{II}}(\text{CN})_5(\text{NH}_3)]_{1/4}\}$  (**CuFe-H<sub>2</sub>O**) and  $[\text{Cu}^{\text{II}}(\text{H}_2\text{O})_3]_2[\text{Fe}^{\text{II}}(\text{CN})_6]$  (**CuFe**) at (a) pH 6.0 and (b) pH 8.3.

Fe) and *p*-NPP (25 mM). The conversion ratios in 24 h and  $v_0$  values for  $[\text{Cu}^{\text{II}}(\text{H}_2\text{O})_x]_y\{[\text{Fe}^{\text{II}}(\text{CN})_5(\text{NH}_3)]_n[\text{Fe}^{\text{II}}(\text{CN})_6]_{1-n}\}$  complexes (22% and  $0.4 \times 10^{-3} \text{ mol L}^{-1} \text{ h}^{-1}$  for  $n = 0.50$ , and 34% and  $1.2 \times 10^{-3} \text{ mol L}^{-1} \text{ h}^{-1}$  for  $n = 0.83$ ) were higher than those for **CuFe** ( $n = 0$ )

but lower than those for **CuFe-NH<sub>3</sub>** ( $n = 1$ ), suggesting that increasing the number of Fe<sup>II</sup> ions with single open sites in the PBAs is important to achieve high catalytic activity (Figure 8).

## CONCLUSION

CN-deficient Prussian blue analogues (PBAs),  $[M^N(H_2O)_x]_y[Fe^{II}(CN)_5(NH_3)]$  (**MFe-NH<sub>3</sub>**,  $M^N = Cu^{II}$ ,  $Co^{II}$  or  $Ga^{III}$ ), were synthesized to examine C-bound Fe<sup>II</sup> ions with single open sites as

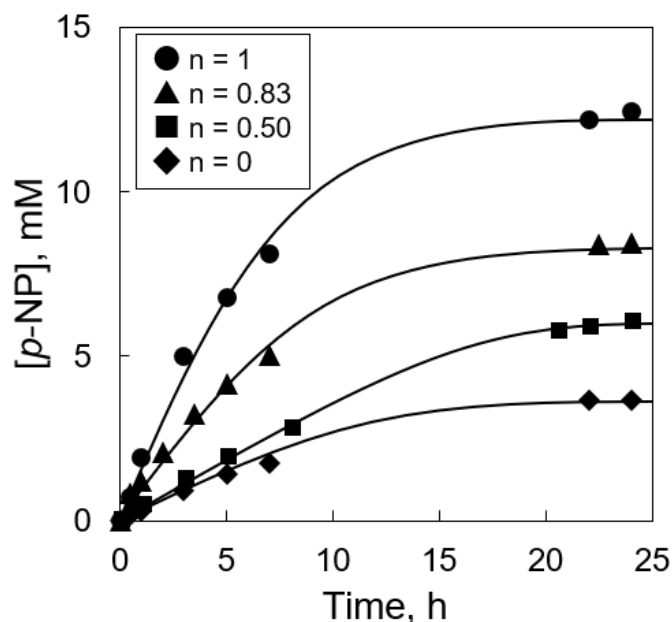


**Figure 8.** Time profiles of the *p*-nitrophenolate ion (*p*-NP) formation in a HEPES buffer solution (100 mM, 0.75 mL, pH 6.0, 50 °C) containing disodium *p*-nitrophenyl phosphate (*p*-NPP, 25 mM) in the presence of  $[Cu^{II}(H_2O)_x]_y\{[Fe^{II}(CN)_5(NH_3)]_n[Fe^{II}(CN)_6]_{1-n}\}$  complexes ( $n = 0, 0.50, 0.83$  or  $1$ ).

precisely controlled active species for hydrolysis of *p*-nitrophenyl phosphate. Liberation of NH<sub>3</sub> from the Fe<sup>II</sup> ions during the catalytic reactions resulted in the formation of exactly single open site on each Fe<sup>II</sup> ion, different from conventional PBAs. High catalytic activity of Fe<sup>II</sup> ions with open sites coupled with catalytically inert Cu<sup>II</sup> ions as the M<sup>N</sup> ions clearly indicated the direct

involvement of the Fe<sup>II</sup> ions as the active species in the catalytic hydrolysis. Then, heterogeneous catalysis of the CN-deficient PBAs employing Co<sup>II</sup> and Ga<sup>III</sup> ions, which are catalytically active species in conventional PBAs, instead of Cu<sup>II</sup> ions was examined. However, no catalysis enhancement was observed for the CN-deficient PBAs containing Co<sup>II</sup> and Ga<sup>III</sup>, because Lewis acidity of the Fe<sup>II</sup> ions enhanced by the M<sup>N</sup> ions favors interaction with hydrogen phosphate and/or ammine ligand. These results suggest that heterogeneous catalysis of metal ions with precisely controlled open sites can be tuned by interaction between coupled metal ions in CN-deficient PBAs, leading to rational design of active sites for highly sophisticated heterogeneous catalysis.

#### ASSOCIATED CONTENT

**Supporting Information.** The Supporting Information is available free of charge on the ACS Publications website. Scanning electron microscope (SEM) images, X-ray fluorescence spectra, X-ray photoelectron spectra (XPS), nitrogen (N<sub>2</sub>) adsorption-desorption isotherms, infrared (IR) spectra, ultraviolet-visible (UV-Vis) spectra, powder X-ray diffraction (PXRD) patterns, reaction profiles, elemental analyses data.

#### AUTHOR INFORMATION

##### **Corresponding Author**

\*E-mail: ymd@a-chem.eng.osaka-cu.ac.jp.

##### **Author Contributions**

The manuscript was written through contributions of all authors. All authors have given approval to the final version of the manuscript.

## Funding Sources

This work was supported by Innovative Science and Technology Initiative for Security (ATLA, Japan) to Y. Y. (Nos. JPJ161000157 and JPJ191047001), JSPS KAKENHI to Y. Y. (No. JP16H02268) and to H. T. (Nos. JP19K15591 and JP20H05110), the Koyanagi Foundation and the Paloma Environmental Technology Development Foundation.

## Notes

The authors declare no competing financial interests.

## REFERENCES

- (1) Chen, X.; Lyu, Y. H.; Wang, Z. Y.; Qiao, X.; Gates, B. C.; Yang, D., Tuning  $Zr_{12}O_{22}$  Node Defects as Catalytic Sites in the Metal–Organic Framework hcp UiO-66. *ACS Catal* **2020**, *10*, 2906–2914.
- (2) Wang, W. J.; Sharapa, D. I.; Chandresh, A.; Nefedov, A.; Heißler, S.; Heinke, L.; Studt, F.; Wang, Y. M.; Wöll, C., Interplay of Electronic and Steric Effects to Yield Low-Temperature CO Oxidation at Metal Single Sites in Defect-Engineered HKUST-1. *Angew. Chem. Int. Ed.* **2020**, *59*, 10514–10518.
- (3) Feng, X.; Hajek, J.; Jena, H. S.; Wang, G. B.; Veerapandian, S. K. P.; Morent, R.; De Geyter, N.; Leyssens, K.; Hoffman, A. E. J.; Meynen, V.; Marquez, C.; De Vos, D. E.; Van Speybroeck, V.; Leus, K.; Van Der Voort, P., Engineering a Highly Defective Stable UiO-66 with Tunable Lewis- Brønsted Acidity: The Role of the Hemilabile Linker. *J. Am. Chem. Soc.* **2020**, *142*, 3174–3183.
- (4) Yang, D.; Gaggioli, C. A.; Ray, D.; Babucci, M.; Gagliardi, L.; Gates, B. C., Tuning Catalytic Sites on  $Zr_6O_8$  Metal–Organic Framework Nodes via Ligand and Defect Chemistry



Probed with *tert*-Butyl Alcohol Dehydration to Isobutylene. *J. Am. Chem. Soc.* **2020**, *142*, 8044–8056.

(5) Epp, K.; Luz, I.; Heinz, W. R.; Rapeyko, A.; Llabrés i Xamena, F. X.; Fischer, R. A., Defect-Engineered Ruthenium MOFs as Versatile Heterogeneous Hydrogenation Catalysts. *ChemCatChem* **2020**, *12*, 1720–1725.

(6) Yadav, A.; Kanoo, P., Metal-Organic Frameworks as Platform for Lewis-Acid-Catalyzed Organic Transformations. *Chem. Asian J.* **2019**, *14*, 3531–3551.

(7) Xu, C. P.; Fang, R. Q.; Luque, R.; Chen, L. Y.; Li, Y. W., Functional Metal-Organic Frameworks for Catalytic Applications. *Coord. Chem. Rev.* **2019**, *388*, 268–292.

(8) Wu, Y. J.; Wang, C. Y., Insight into the Catalytic Effects of Open Metal Sites in Metal-Organic Frameworks on Hydride Dehydrogenation via Nanoconfinement. *ACS Sustain. Chem. Eng.* **2019**, *7*, 16013–16025.

(9) Heinz, W. R.; Kratky, T.; Drees, M.; Wimmer, A.; Tomanec, O.; Gunther, S.; Schuster, M.; Fischer, R. A., Mixed Precious-Group Metal-Organic Frameworks: A Case Study of the HKUST-1 Analogue  $[\text{Ru}_x\text{Rh}_{3-x}(\text{BTC})_2]$ . *Dalton Trans.* **2019**, *48*, 12031–12039.

(10) Tabe, H.; Matsushima, M.; Tanaka, R.; Yamada, Y., Creation and Stabilisation of Tuneable Open Metal Sites in Thiocyanato-Bridged Heterometallic Coordination Polymers to Be Used as Heterogeneous Catalysts. *Dalton Trans.* **2019**, *48*, 17063–17069.

(11) Wen, Y. H.; Zhang, J.; Xu, Q.; Wu, X. T.; Zhu, Q. L., Pore Surface Engineering of Metal-Organic Frameworks for Heterogeneous Catalysis. *Coord. Chem. Rev.* **2018**, *376*, 248–276.

- (12) Liang, W. B.; Li, L.; Hou, J. W.; Shepherd, N. D.; Bennett, T. D.; D'Alessandro, D. M.; Chen, V., Linking Defects, Hierarchical Porosity Generation and Desalination Performance in Metal-Organic Frameworks. *Chem. Sci.* **2018**, *9*, 3508–3516.
- (13) Kirchon, A.; Feng, L.; Drake, H. F.; Joseph, E. A.; Zhou, H. C., From Fundamentals to Applications: A Toolbox for Robust and Multifunctional MOF Materials. *Chem. Soc. Rev.* **2018**, *47*, 8611–8638.
- (14) Dhakshinamoorthy, A.; Li, Z. H.; Garcia, H., Catalysis and Photocatalysis by Metal Organic Frameworks. *Chem. Soc. Rev.* **2018**, *47*, 8134–8172.
- (15) DeStefano, M. R.; Islamoglu, T.; Garibay, S. J.; Hupp, T. H.; Farha, O. K. Room-Temperature Synthesis of UiO-66 and Thermal Modulation of Densities of Defect Sites. *Chem. Mater.* **2017**, *29*, 1357–1361.
- (16) Gutov, O. V.; Hevia, M. G.; Escudero-Adán, E. C.; Shafir, A., Metal-Organic Framework (MOF) Defects Under Control: Insights into the Missing Linker Sites and Their Implication in the Reactivity of Zirconium-Based Frameworks. *Inorg. Chem.* **2015**, *54*, 8396–8400.
- (17) Fang, Z. L.; Bueken, B.; De Vos, D. E.; Fischer, R. A., Defect-Engineered Metal-Organic Frameworks. *Angew. Chem. Int. Ed.* **2015**, *54*, 7234–7254.
- (18) Wu, H.; Chua, Y. S.; Krungleviciute, V.; Tyagi, M.; Chen, P.; Yildirim, T.; Zhou, W. Unusual and Highly Tunable Missing-Linker Defects in Zirconium Metal–Organic Framework UiO-66 and Their Important Effects on Gas Adsorption. *J. Am. Chem. Soc.* **2013**, *135*, 10525–10532.
- (19) Matsunaga, S.; Hasada, K.; Sugiura, K.; Kitamura, N.; Kudo, Y.; Endo, N.; Mori, W., Hetero Bi-Paddle-Wheel Coordination Networks: A New Synthetic Route to Rh-Containing Metal-Organic Frameworks. *Bull. Chem. Soc. Jpn.* **2012**, *85*, 433–438.

- (20) Marx, S.; Kleist, W.; Baiker, A., Synthesis, Structural Properties, and Catalytic Behavior of Cu-BTC and Mixed-linker Cu-BTC-PyDC in the Oxidation of Benzene Derivatives. *J. Catal.* **2011**, *281*, 76–87.
- (21) Horike, S.; Dincă, M.; Tamaki, K.; Long, J. R., Size-Selective Lewis Acid Catalysis in a Microporous Metal-Organic Framework with Exposed  $Mn^{2+}$  Coordination Sites. *J. Am. Chem. Soc.* **2008**, *130*, 5854–5855.
- (22) Zhang, W.; Kauer, M.; Halbherr, O.; Epp, K.; Guo, P.; Gonzalez, M. I.; Xiao, D. J.; Wiktor, C.; Llabrés i Xamena, F. X.; Wöll, C.; Wang, Y.; Muhler, M.; Fischer, R. A., Ruthenium Metal–Organic Frameworks with Different Defect Types: Influence on Porosity, Sorption, and Catalytic Properties, *Chem. Eur. J.* **2016**, *22*, 14297–14307.
- (23) Kozachuk, O.; Luz, I.; Llabrés i Xamena, F. X.; Noei, H.; Kauer, M.; Albada, H. B.; Bloch, E. D.; Marler, B.; Wang, Y. M.; Muhler, M.; Fischer, R. A., Multifunctional, Defect-Engineered Metal-Organic Frameworks with Ruthenium Centers: Sorption and Catalytic Properties. *Angew. Chem. Int. Ed.* **2014**, *53*, 7058–7062.
- (24) Guari, Y.; Larionova, J., *Prussian Blue-Type Nanoparticles and Nanocomposites: Synthesis, Devices, and Applications, 1st ed.* Jenny Stanford Publishing: Singapore, 2019.
- (25) Itaya, K.; Uchida, I.; Neff, V. D., Electrochemistry of Polynuclear Transition Metal Cyanides: Prussian Blue and Its Analogs. *Acc. Chem. Res.* **1986**, *19*, 162–168.
- (26) Herren, F.; Fischer, P.; Ludi, A.; Halg, W., Neutron Diffraction Study of Prussian Blue,  $Fe_4[Fe(CN)_6]_3 \cdot xH_2O$ . Location of Water Molecules and Long-Range Magnetic Order. *Inorg. Chem.* **1980**, *19*, 956–959.
- (27) Buser, H. J.; Schwarzenbach, D.; Petter, W.; Ludi, A., The Crystal Structure of Prussian Blue:  $Fe_4[Fe(CN)_6]_3 \cdot xH_2O$ . *Inorg. Chem.* **1977**, *16*, 2704–2710.

- (28) Tabe, H.; Terashima, C.; Yamada, Y. Effect of Surface Acidity of Cyano-Bridged Polynuclear Metal Complexes on the Catalytic Activity for the Hydrolysis of Organophosphates. *Catal. Sci. Technol.* **2018**, *8*, 4747–4756.
- (29) Ishizaki, M.; Fujii, H.; Toshima, K.; Tanno, H.; Sutoh, H.; Kurihara, M., Preparation of Co-Fe Oxides Immobilized on Carbon Paper Using Water-Dispersible Prussian-Blue Analog Nanoparticles and Their Oxygen Evolution Reaction (OER) Catalytic Activities. *Inorg. Chim. Acta.* **2020**, *502*, 119345.
- (30) Ghobadi, T. G. U.; Ghobadi, A.; Buyuktemiz, M.; Yildiz, E. A.; Yildiz, D. B.; Yaglioglu, H. G.; Dede, Y.; Ozbay, E.; Karadaş, F., A Robust, Precious-Metal-Free Dye-Sensitized Photoanode for Water Oxidation: A Nanosecond-Long Excited State Lifetime through a Prussian Blue Analogue. *Angew. Chem. Int. Ed.* **2020**, *59*, 4082–4090.
- (31) Cao, L. M.; Lu, D.; Zhong, D. C.; Lu, T. B., Prussian Blue Analogues and Their Derived Nanomaterials for Electrocatalytic Water Splitting. *Coord. Chem. Rev.* **2020**, *407*, 213156.
- (32) Zhao, C. X.; Liu, B.; Li, X. N.; Zhu, K. X.; Hu, R. S.; Ao, Z. M.; Wang, J. H., A Co-Fe Prussian Blue Analogue for Efficient Fenton-Like Catalysis: The Effect of High-Spin Cobalt. *Chem. Commun.* **2019**, *55*, 7151–7154.
- (33) Pires, B. M.; dos Santos, P. L.; Katic, V.; Strohauser, S.; Landers, R.; Formiga, A. L. B.; Bonacin, J. A., Electrochemical Water Oxidation by Cobalt-Prussian Blue Coordination Polymer and Theoretical Studies of the Electronic Structure of the Active Species. *Dalton Trans.* **2019**, *48*, 4811–4822.
- (34) Feng, Y.; Han, H.; Kim, K. M.; Dutta, S.; Song, T., Self-templated Prussian blue analogue for efficient and robust electrochemical water oxidation. *J. Catal.* **2019**, *369*, 168–174.

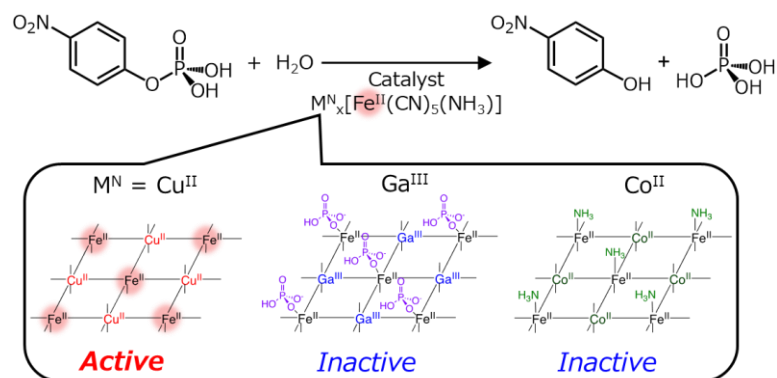
- (35) Marquez, C.; Cirujano, F. G.; Van Goethem, C.; Vankelecom, I.; De Vos, D. E.; De Baerdemaeker, T. Tunable Prussian Blue Analogues for the Selective Synthesis of Propargylamines Through  $A^3$  Coupling. *Catal. Sci. Technol.* **2018**, *8*, 2061–2065.
- (36) Gao, Q. L.; Chen, J.; Li, Q.; Zhang, J.; Zhai, Z.; Zhang, S. T.; Yu, R. B.; Xing, X. R. Structure and Excellent Visible Light Catalysis of Prussian Blue Analogues  $BiFe(CN)_6 \cdot 4H_2O$ . *Inorg. Chem. Front.* **2018**, *5*, 438–445.
- (37) Alsac, E. P.; Ulker, E.; Nune, S. V. K.; Dede, Y.; Karadaş, F. Tuning the Electronic Properties of Prussian Blue Analogues for Efficient Water Oxidation Electrocatalysis: Experimental and Computational Studies. *Chem. Eur. J.* **2018**, *24*, 4856–4863.
- (38) Zou, H. H.; Yuan, C. Z.; Zou, H. Y.; Cheang, T. Y.; Zhao, S. J.; Qazi, U. Y.; Zhong, S. L.; Wang, L.; Xu, A. W. Bimetallic Phosphide Hollow Nanocubes Derived from a Prussian-Blue-Analog Used as High-Performance Catalysts for the Oxygen Evolution Reaction. *Catal. Sci. Technol.* **2017**, *7*, 1549–1555.
- (39) Zakaria, M. B.; Chikyow, T., Recent Advances in Prussian Blue and Prussian Blue Analogues: Synthesis and Thermal Treatments. *Coord. Chem. Rev.* **2017**, *352*, 328–345.
- (40) Li, X. N.; Liu, J. Y.; Rykov, A. I.; Han, H. X.; Jin, C. Z.; Liu, X.; Wang, J. H. Excellent photo-Fenton Catalysts of Fe–Co Prussian Blue Analogues and Their Reaction Mechanism Study. *Appl. Catal. B* **2015**, *179*, 196–205.
- (41) Pintado, S.; Goberna-Ferrón, S.; Escudero-Adán, E. C.; Galán-Mascarós, J. R. Fast and Persistent Electrocatalytic Water Oxidation by Co–Fe Prussian Blue Coordination Polymers. *J. Am. Chem. Soc.* **2013**, *135*, 13270–13273.

- (42) Tabe, H.; Kitase, A.; Yamada, Y., Utilization of Core-Shell Nanoparticles to Evaluate Subsurface Contribution to Water Oxidation Catalysis of  $[\text{Co}^{\text{II}}(\text{H}_2\text{O})_2]_{1.5}[\text{Co}^{\text{III}}(\text{CN})_6]$  nanoparticles. *Appl. Catal. B* **2020**, *262*, 118101.
- (43) Aratani, Y.; Suenobu, T.; Ohkubo, K.; Yamada, Y.; Fukuzumi, S., Dual Function Photocatalysis of Cyano-Bridged Heteronuclear Metal Complexes for Water Oxidation and Two-Electron Reduction of Dioxygen to Produce Hydrogen Peroxide as a Solar Fuel. *Chem. Commun.* **2017**, *53*, 3473–3476.
- (44) Yamada, Y.; Oyama, K.; Suenobu, T.; Fukuzumi, S., Photocatalytic Water Oxidation by Persulphate with a  $\text{Ca}^{2+}$  Ion-Incorporated Polymeric Cobalt Cyanide Complex Affording  $\text{O}_2$  with 200% Quantum Efficiency. *Chem. Commun.* **2017**, *53*, 3418–3421.
- (45) Isaka, Y.; Oyama, K.; Yamada, Y.; Suenobu, T.; Fukuzumi, S. Photocatalytic Production of Hydrogen Peroxide from Water and Dioxygen Using Cyano-Bridged Polynuclear Transition Metal Complexes as Water Oxidation Catalysts. *Catal. Sci. Technol.* **2016**, *6*, 681–684.
- (46) Yamada, Y.; Oyama, K.; Gates, R.; Fukuzumi, S. High Catalytic Activity of Heteropolynuclear Cyanide Complexes Containing Cobalt and Platinum Ions: Visible-Light Driven Water Oxidation. *Angew. Chem. Int. Ed.* **2015**, *54*, 5613–5617.
- (47) Yamada, Y.; Yoneda, M.; Fukuzumi, S. A Robust One-Compartment Fuel Cell with a Polynuclear Cyanide Complex as a Cathode for Utilizing  $\text{H}_2\text{O}_2$  as a Sustainable Fuel at Ambient Conditions. *Chem. Eur. J.* **2013**, *19*, 11733–11741.
- (48) Takahashi, A.; Tanaka, H.; Parajuli, D.; Nakamura, T.; Minami, K.; Sugiyama, Y.; Hakuta, Y.; Ohkoshi, S.; Kawamoto, T. Historical Pigment Exhibiting Ammonia Gas Capture beyond Standard Adsorbents with Adsorption Sites of Two Kinds. *J. Am. Chem. Soc.* **2016**, *138*, 6376–6379.

- (49) Aksoy, M.; Nune, S. V. K.; Karadaş, F. A. Novel Synthetic Route for the Preparation of an Amorphous Co/Fe Prussian Blue Coordination Compound with High Electrocatalytic Water Oxidation Activity. *Inorg. Chem.* **2016**, *55*, 4301–4307.
- (50) Yeste, M. P.; Vidal, H.; García-Cabeza, A. L.; Hernández-Garrido, J. C.; Guerra, F. M.; Cifredo, G. A.; González-Leal, J. M.; Gatica, J. M. *Appl. Catal. A* **2017**, *552*, 58–69.
- (51) Ghobadi, T. G. U.; Yildiz, E. A.; Buyuktemiz, M.; Akbari, S. S.; Topkaya, D.; İsci, Ü.; Dede, Y.; Yaglioglu, H. G.; Karadas, F. *Angew. Chem. Int. Ed.* **2018**, *57*, 17173–17177.
- (52) Nakamoto, K. *Infrared and Raman Spectra of Inorganic and Coordination Compounds*; 4th ed. John Wiley & Sons: NY, 1986.
- (53) Kandanapitiye, M. S.; Valley, B.; Yang, L. D.; Fry, A. M.; Patrick M. Woodward, P. M.; Huang, S. D. Gallium Analogue of Soluble Prussian Blue  $\text{KGa}[\text{Fe}(\text{CN})_6] \cdot n\text{H}_2\text{O}$ : Synthesis, Characterization, and Potential Biomedical Applications. *Inorg. Chem.* **2013**, *52*, 2790–2792.
- (54) Parajuli, D.; Noguchi, H.; Takahashi, A.; Tanaka, H.; Kawamoto, T. Prospective Application of Copper Hexacyanoferrate for Capturing Dissolved Ammonia. *Ind. Eng. Chem. Res.* **2016**, *55*, 6708–6715.
- (55) Ahmed, A. A.; Gypser, S.; Leinweber, P.; Freese, D.; Kuhn, O. Infrared Spectroscopic Characterization of Phosphate Binding at the Goethite-Water Interface. *Phys. Chem. Chem. Phys.* **2019**, *21*, 4421–4434.
- (56) Tejedor-Tejedor, M. I.; Anderson, M. A., Protonation of Phosphate on the Surface of Goethite as Studied by CIR-FTIR and Electrophoretic Mobility. *Langmuir* **1990**, *6*, 602–611.

For Table of Contents Only

TOC graphic



Synopsis

Single open sites were created on  $\text{Fe}^{\text{II}}$  ions of CN-deficient Prussian blue analogues,  $[\text{M}^{\text{N}}(\text{H}_2\text{O})_x]_y[\text{Fe}^{\text{II}}(\text{CN})_5(\text{NH}_3)]$ ;  $\text{M}^{\text{N}} = \text{Cu}^{\text{II}}$ ,  $\text{Co}^{\text{II}}$  or  $\text{Ga}^{\text{III}}$ ) by liberation of  $\text{NH}_3$  ligand. Lewis acidity of the  $\text{Fe}^{\text{II}}$  ions tuned by the  $\text{M}^{\text{N}}$  ions through metal-metal interaction affected interaction between the  $\text{Fe}^{\text{II}}$  ions and  $\text{HPO}_4^-$  or  $\text{NH}_3$  ligands, resulting in enhancement of heterogeneous catalysis for hydrolysis of toxic organophosphates.